A 4 V Operation, Flexible Braille Display Using Organic Transistors, Carbon Nanotube Actuators, and Organic Static Random-Access Memory

*Kenjiro Fukuda, Tsuyoshi Sekitani, Ute Zschieschang, Hagen Klauk, Kazunori Kuribara, Tomoyuki Yokota, Takushi Sugino, Kinji Asaka, Masaaki Ikeda, Hirokazu Kuwabara, Tatsuya Yamamoto, Kazuo Takimiya, Takanori Fukushima, Takuzo Aida, Makoto Takamiya, Takayasu Sakurai, and Takao Someya**

A sheet-type Braille display operating at 4 V has been successfully fabricated by integrating organic an static random-access memory (SRAM) array with carbon nanotube (CNT)-based actuators that are driven by organic thin-film transistors (control-TFTs). The on current of organic control-TFTs that drive CNT actuators exceeds 3 mA, the mobility exceeds 1 $cm^2 V^{-1}s^{-1}$, and the on/off ratio exceeds 10^5 at an operational voltage of 3 V. By adjusting the process time for the formation of the aluminum oxide dielectrics, the threshold voltage of the organic TFTs can be systematically controlled. This technique leads to an improved static noise margin of the SRAM and enables its stable operation with a short programming time of 2 ms at a programming voltage of 2 V. As a demonstration of the operation of one actuator with one control-TFT and SRAM: the displacement of actuator exceeds 300 μm at an operation voltage of 4 V, which is large enough for a blind person to recognize the pop-up of braille dots. Integrating the SRAM array reduces the frame rate of a 12 dot × 12 dot display from 1/21.6 s to 1/2.9 s.

1. Introduction

Large-area electronics are key technologies for realizing ambient electronics that are expected to support our safety and security of life. Organic semiconductors have attracted much attention because they can be processed on plastic substrates and by printing fabrication techniques at room temperature. These features allow large-area and flexible applications of organic semiconductors, including solar cells,[1] thin-film transistors (TFTs),[2] sensors,[3] or memory devices[4–10] Although large-area actuators are required for enhancing electrical functionalities of large-area electronics in combination with large-area sensors, only a few applications of

Dr. K. Fukuda,[+] K. Kuribara, T. Yokota, T. Sakurai, Prof. T. Someya
Department of Applied Physics
The University of Tokyo
7-3-1 Hongo, Bunkyo-ku, Tokyo 113-8656, Japan
E-mail: someya@ee.t.u-tokyo.ac.jp
Prof. T. Sekitani, Prof. T. Someya
Department of Electrical and Electronic Engineering
The University of Tokyo
7-3-1 Hongo, Bunkyo-ku, Tokyo 113-8656, Japan
Dr. U. Zschieschang, Dr. H. Klauk
Max Planck Institute for Solid State Research
Heisenbergstr. 1, 70569 Stuttgart, Germany
Dr. T. Sugino, Dr. K. Asaka
Research Institute for Cell Engineering
National Institute of Advanced Industrial Science and Technology (AIST)
Midorigaoka 1-8-31, Ikeda, Osaka 563-8577, Japan
Dr. M. Ikeda, Dr. H. Kuwabara
Functional Chemicals R&D Laboratories
Nippon Kayaku Co., Ltd. 3-26-8, Shimo, Kita-ku, Tokyo, 115-8588, Japan
Dr. T. Yamamoto, Prof. K. Takimiya
Department of Applied Chemistry
Hiroshima University
1-4-1, Kagamiyama, Higashi-Hiroshima, Hiroshima, 739-8527, Japan
Prof. T Fukushima
Functional Soft Matter Engineering Laboratory
Advanced Science Institute
RIKEN, 2-1 Hirosawa,Wako, Saitama, 351-0198, Japan
Prof. T. Aida
Department of Chemistry and Biotechnology
The University of Tokyo
7-3-1, Hongo, Bunkyo-ku, Tokyo, 113-8656, Japan
Prof. M. Takamiya
VLSI Design & Education Center
The University of Tokyo
4-6-1, Komaba, Meguro-ku, Tokyo, 153-8505, Japan
Prof. T. Sakurai
Institute of Industrial Science
The University of Tokyo
4-6-1, Komaba, Meguro-ku, Tokyo, 153-8505, Japan
Prof. T. Someya
Institute for Nano Quantum Information Electronics
The University of Tokyo,
4-6-1, Komaba, Meguro-ku, Tokyo, 153-8505, Japan
Prof. T. Someya
Core Research for Evolutional Science and Technology
Sanban-cho Bldg, 4F, 5, Sanban-cho
Chiyoda-ku, Tokyo, 102-0075, Japan
[+]Present address: Research Center for Organic Electronics, Yamagata University, 4-3-16, Jonan, Yonezawa, Yamagata, 992-8510, Japan

DOI: 10.1002/adfm.201101050

soft actuators have been reported, so far.[11] Our group has previously fabricated sheet-type Braille displays by integrating organic TFTs and soft polymer actuators.[12] However, these displays reported in the past required a large operation voltage; more than 40 V for driving polymer actuators using Au-plated Nafion. An actuation time of more than 1 s is required for operating one actuator and achieving displacements of more than 300 μm, which is necessary to recognize whether the individual Braille dots are up or down. Furthermore, the most difficult obstacle for practical applications is the device instability in ambient conditions. In fact, the Nafion actuators require sufficiently moist conditions for the actuation,[13] while organic semiconductors are degraded by atmospheric components including O_2 or H_2O[14]

Recently, air-stable actuators comprising carbon nanotubes (CNTs) dispersed in polymers have been reported by Fukushima et al., which exhibit large displacements (5 mm) and high-speed actuation a low operating voltages (≈3–4 V).[15]

The integration of organic TFTs with CNT-based actuators to realize low-operation, air-stable Braille displays faces three technical challenges on material, process, and circuit engineering aspects. One is to decrease the operation voltages of organic TFTs for direct driving CNT-based actuators. A second one is to supply large source–drain currents of the order of milliamperes from TFTs operating at 4 V, because CNT-based actuators require large currents for achieving large displacements. The third is to develop and integrate an organic static random-access memory (SRAM) array with actuators for driving all actuators at the same time, and then to increase the frame rate (that is, improve the refresh speed) of Braille displays.

Lowering the operation voltage of organic TFTs has been reported using novel gate dielectrics with a large capacitance per unit area. Among the approaches are the use of ultrathin insulating polymers,[16,17] self-assembled nanodielectrics,[18,19] high-dielectric constant (high-*k*) metal oxide layers,[20,21] and electric double-layer capacitors.[22] Another approach is the use of a gate dielectric composed of a thin, plasma-grown aluminum oxide (AlO_x) layer in combination with an alkylphosphonic acid self-assembled monolayer (SAM), which has shown good performance as well as sufficient yield to allow the realization of organic large-scale integrated (LSI) circuits.[10,23–27]

In order to increase the frame rate of the Braille display, the organic memory is required.[28] In this application, the critical feature required for organic memories is not non-volatility or high density but a faster programming speed and low-voltage operation. When an organic SRAM matrix with a programming speed of 40 ms was integrated with a sheet-type Braille display, the frame rate of a 6 × 4 character (144 dots) Braille display was increased from 0.002 Hz to 0.6 Hz.[28] However, the operation voltage of the organic SRAM in our previous demonstration was 40 V or more, which is too large for practical applications.[12] Thus, a significant reduction in operating voltage is highly desirable for power-consumption and safety reasons.

However, simply applying organic TFTs with standard AlO_x/SAM gate dielectrics to reduce the operation voltage of SRAM cells is not straightforward, because SRAM designs that utilize only p-channel transistors (as opposed to p-channel and n-channel transistors) require deterministic control of the threshold voltage of the transistors. The reason is that SRAM cells are functional only if they utilize depletion-mode ("normally-on") transistors (e.g., p-channel transistors with a positive threshold voltage) but not if the transistors are enhancement-mode ("normally-off", such as p-channel transistors with negative threshold voltage). However, most of the previously reported organic TFTs with AlO_x/SAM gate dielectric show enhancement-mode behavior, and practical methods to control the threshold voltage of low-voltage organic TFTs have only very recently been reported.[29]

In this paper, we fabricated a Braille sheet displays operating at 4 V by integrating organic TFT drivers, organic SRAMs, and CNT-based actuators. The displacement and the generating force of the CNT-based actuators can be controlled systematically by changing the thickness of the electrodes. The combination of oxygen-plasma-grown AlO_x and *n*-tetradecylphosphonic acid SAMs was used for the gate dielectrics, while dinaphtho-[2,3-b:2′,3′-f]thieno[3,2-b]thiophene (DNTT)[30,31] was used as the organic semiconductor to realize air-stable, high-performance p-channel organic TFTs. We found that the threshold voltage of the transistors depends on how long the aluminum gate electrodes are exposed to an oxygen plasma in order to form the AlO_x layer, which - together with the alkylphosphonic acid SAM – forms the gate dielectric of the organic TFTs. We found that the threshold voltage can be changed systematically from –0.57 to +0.10 V by extending the plasma time from 1 to 30 min. For manufacturing organic TFT drivers, a mobility of 1.0 $cm^2\ V^{-1}s^{-1}$ is achieved, the ON/OFF ratio exceeds 10^6, and the on current is 4.9 mA at 3 V. For an organic SRAM the programming speed can be reduced to 1.5 ms at 2 V by reducing the channel length down to 20 μm and using DNTT as p-type organic semiconductors. For operating actuator with organic control TFTs and SRAM, the time required to drive a displacement of more than 300 μm was 2.9 s at –4.5 V, which is sufficient for applying this technology to Braille displays.

2. Results

2.1. Carbon Nanotube-Based Actuators

The Braille actuators consist of an electrolyte layer sandwiched between two CNT electrode layers, as shown in **Figure 1**a. In this study, each CNT-based actuator can be operated selectively using the organic TFT matrix, as shown in Figure 1a. The actuator sheet is integrated on the organic TFT matrix sheet (Figure 1b).

A schematic representation of the manufacturing process is shown in the Supporting Information, Figure S1. For the CNT–based actuator, single-walled CNTs (purified Hipco, Carbon Nanotechnologies Inc.), ionic liquid of 1-ethyl-3methylimidazolium tetrafluoroborate ($EMIBF_4$, Fluka), and fluoride-cohexafluoropropylene (PVDF-HFP, Kynar Flex 2801, Arkema Chemicals Inc.) were used. *N*,*N*-dimethylacetamide (DMAc, 99.0%, Kishida Chem. Co.), 4-methyl-2-pentanone (MP, ≥99.5%, Sigma–Aldrich), and propylene carbonate anhydrous (PC, 99.7%, Sigma–Aldrich) were used as solvents.

The Braille actuators consist of an electrolyte layer sandwiched between two CNT electrode layers. The electrode layers were prepared from a mixture of 50 mg single-walled carbon

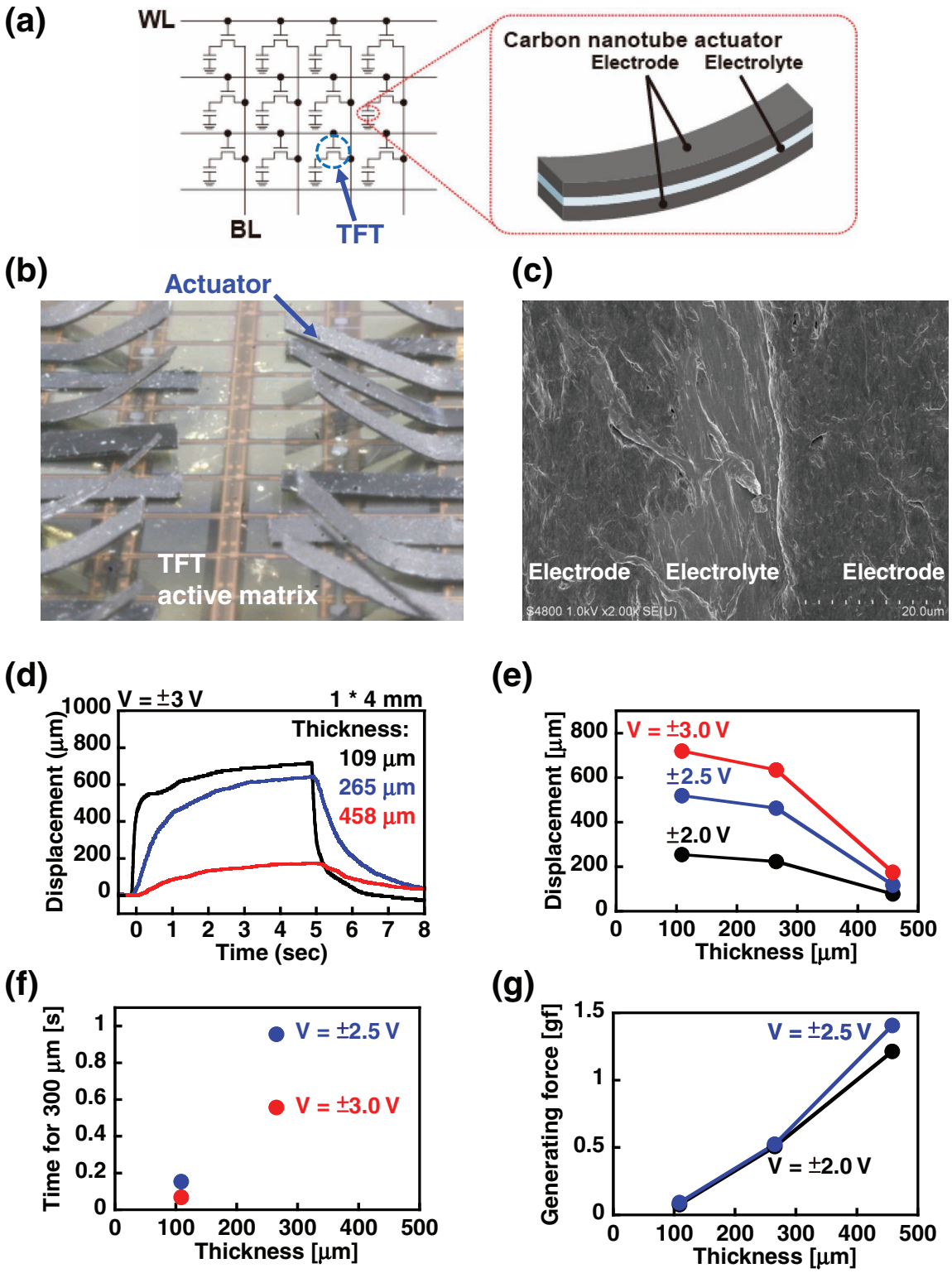

Figure 1. CNT-based actuators: a) Circuit diagrams of CNT-based actuators with organic TFTs operating at low voltages. b) Photograph of the CNT-based actuators operated by the organic TFTs. Each actuator is operated by the organic TFT cell below the actuator sheet. c) Cross-sectional scanning electron microscopy image of the CNT-based actuator. d) Displacement of the actuator as a function of time (Black: thickness of 109 μm; blue: thickness of 265 μm; red: thickness of 458 μm). The size of the actuators is 1 mm × 4 mm. Operation voltage: ±3.0 V. e) Displacement of the actuators as a function of total thickness (black: operation voltage of ±2.0 V; blue: operation voltage of ±2.5 V; red: operation voltage of ±3.0 V). f) Time required to drive a displacement of more than 300 μm as a function of total thickness of the actuators (blue: operation voltage of ±2.5 V; red: operation voltage of ±3.0 V). g) Generating force as a function of total thickness of the actuators (black: operation voltage of ±2.0 V; blue: operation voltage of ±2.5 V).

nanotubes, 120 mg of the ionic liquid $EMIBF_4$, and 80 mg PVDF-HFP dissolved in 9 ml DMAc. The mixture was stirred at room temperature for more than 3 d and then sonicated in an ultrasonic bath (36 kHz) for more than 24 h to gelatinize the mixture. 1.6 mL of the gelatinous mixture was then cast onto a Teflon mold (dimensions of 2.5 cm × 2.5 cm) and the solvent was dried for 3 d at 80 °C in a vacuum oven. The thickness of the electrodes changed from 50 to 200 μm by changing the amount of gelatinous mixture to the molds.

The gel electrolyte layers were prepared from a mixture of 100 mg $EMIBF_4$ and 100 mg PVDF-HFP dissolved in 3 mL MP and 250 mg PC. The mixture was stirred at 65 °C in a sand bath. 0.3 mL of the mixture were then cast onto an aluminum mold (2.5 cm × 2.5 cm) and dried for 3 d at 80 °C in a vacuum oven. The thickness of the obtained electrolyte layer was approximately 15 μm.

The three-layer actuator sandwich was fabricated by pressing two CNT electrode layers against an electrolyte film at 70 °C for 90 s. The total thicknesses of the actuators were approximately 100 μm, 200 μm, 400 μm, respectively.

The cross-sectional image of the fabricated actuator was observed by the scanning electron microscopy (SEM; S-4800, Hitachi high-technologies), as shown in Figure 1c and the Supporting Information, Figure S2. Using a thermocompression bonding process, the polymers in the three layers were connected accross the layers and, as a result, a very smooth interface was formed between electrode and electrolyte. This leads to large displacement of the actuator, because ions can easily be moved between electrode and electrolyte.

Figure 1d shows the time-dependent displacement of a directly driven CNT-based actuator with a size of 1 mm × 4 mm. The black, blue, and red lines indicate actuators of 109, 265, and 458 μm thickness, respectively. A square-wave signal with an amplitude of ±3 V and a frequency of 0.1 Hz was applied to the actuator, and the bending motion of the actuator was continuously monitored using a laser displacement meter (KEYENCE, LE-4000) and an oscilloscope (Agilent, DSO6054A). There are significant relations between the displacement or operating speed and the thickness of the actuator. For example, thinner actuator results in a faster speed and larger displacement. Figure 1e shows the displacement of the actuator as a function of the total thickness of the actuators. For the 109 μm thick actuator, a large displacement of about 800 μm was obtained at a voltage of ±3 V. A displacement of 300 μm is demanded for a blind person to recognize, so it is important to estimate the time required to produce a displacement of 300 μm. From the displacement characteristics of the actuators, the time required to produce a displacement of 300 μm was plotted as a function of thickness of the actuators in Figure 1f. CNT actuator with thickness of 109 μm requires displacement time less than 0.1 s. We also measured the generating force of the same actuators, as shown in Figure 1g. At the input voltage of ±2.5 V, the generating force (gf) increased from 0.2 to 1.4 gf and the thickness of the actuator increased from 109 to 458 μm. There is a trade-off between the two important characteristic displacement and generating force, and these results clearly indicate that these important characteristics can be systematically controlled to the demands of electronic applications.

2.2. Manufacture and Electrical Characteristics of Organic Transistors

A Braille display consists of three functional sheets: CNT-based actuators, organic TFTs for driving CNT actuators, and organic TFT-based SRAM. The sheets are laminated to one another using an anisotropic conductive sheet. Since all materials, except from the metal electrodes, are made of organic materials, the entire system is very thin, lightweight, and mechanically flexible (**Figure 2**a). To realize a 4 V Braille display, the organic SRAM array was integrated with CNT-based actuators controlled by high-current organic TFTs, as shown in Figure 2b.

Figure 2c shows a schematic cross-section of a stand-alone organic transistor. First, a 20 nm thick aluminum gate electrode was thermally evaporated through a shadow mask onto

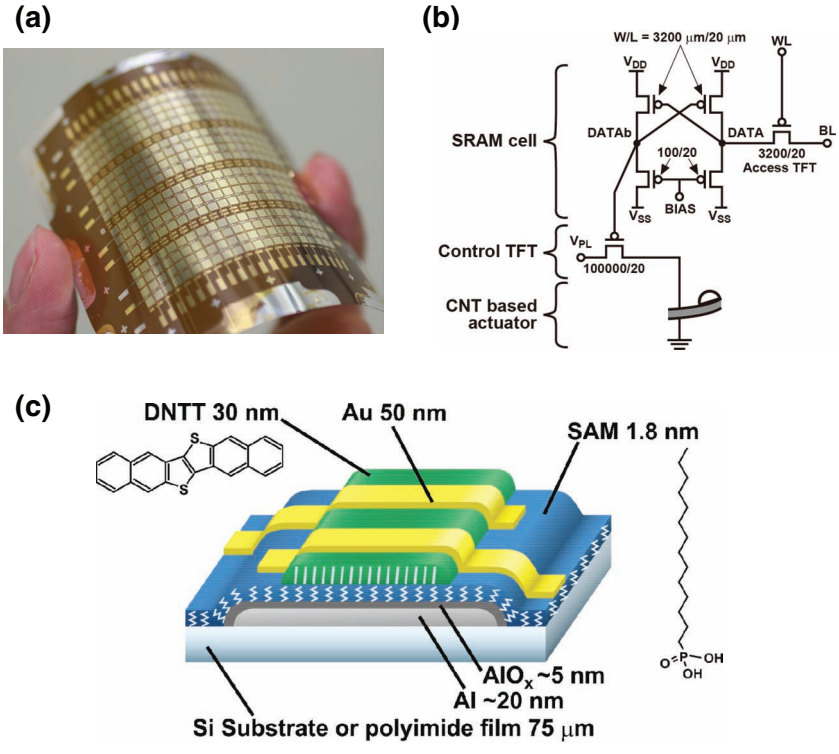

Figure 2. Schematics of fabricated organic transistors: a) Photograph of an organic TFT matrix sheet for operating the Braille display. b) Circuit diagram of one element of the Braille display. c) Schematic cross-section of the organic TFTs) with patterned aluminum gate electrodes, ultrathin aluminum oxide/SAM gate dielectrics, vacuum-deposited organic semiconductor layers (DNTTs), and vacuum-deposited Au source–drain contacts.

a Si reference substrate and/or onto a flexible plastic substrate (UPILEX 75S, Ube Industrial). The gate dielectric layer is composed of a thin layer of aluminum oxide (thickness: 4 nm) and a SAM of *n*-tetradecylphosphonic acid (thickness: 2 nm). The aluminum oxide film was prepared by oxygen-plasma treatment of the Al gate electrodes and provides a high density of hydroxyl groups for adsorption of the self-assembling phosphonic acid molecules. To control the threshold voltage of the TFTs, the duration of the oxygen plasma treatment performed to create the AlO_x layer was controlled between 1 min and 30 min. The plasma power was 300 W. The SAM was prepared by immersing the substrate in a 2-propanol solution of *n*-tetradecylphosphonic acid for 16 h at room temperature.[26,32] The substrates were then rinsed with pure 2-propanol and baked in an oven at 100 °C for 10 min. The organic semiconductor DNTT was deposited in vacuum through a shadow mask to form a 30 nm thick patterned organic semiconductor layer on the gate dielectric. Finally, a 50 nm thick Au layer was evaporated through a shadow mask to form the source–drain contacts. All TFTs have a channel length of 20 µm.

Discrete organic transistors were electrically characterized. Current–voltage characteristics of the TFTs were measured with a semiconductor parameter analyzer (4155C, Agilent Technologies) in ambient conditions. **Figure 3**a shows the transfer characteristics of the DNTT TFTs with different durations of the oxygen plasma treatment performed to create an AlO_x layer (1 min, 3 min, 5 min, 30 min). The drain current, I_D, was measured as a function of the gate-source voltage, V_{GS}, for a drain-source voltage, V_{DS}, of –2 V. For a longer plasma duration the transfer curves shift significantly towards more positive gate-source voltages. The gate-leakage current, I_G, is also shown in Figure 3a. The maximum gate current is less than 100 pA for all transistors. The ON/OFF ratio exceeds 10^6 for all transistors. Figure 3b shows changes in threshold voltage, V_{TH}, and the field-effect mobility in the saturation regime with changing plasma durations. The average threshold voltage of the transistors with a plasma duration of 1 min was –0.57 V, while that of transistors with a plasma duration of 30 min was +0.10 V. The mobility is essentially independent from the plasma duration; the average mobility of the transistors that were exposed to the oxygen plasma for 1 min is 1.0 $cm^2 V^{-1}s^{-1}$, and that of the transistors with a 30 min plasma duration is 0.91 $cm^2 V^{-1}s^{-1}$. This shows that the threshold voltage of the TFTs can be controlled systematically and uniformly by adjusting the plasma duration without degrading the other transistor characteristics, such as the on/off ratio and mobility.

High-current TFTs that control the CNT-based actuators for the Braille display have a channel width of 10 cm (**Figure 4**a). Figure 4b shows the output characteristics of the control TFTs. The drain current (I_D) was measured as a function of V_{DS} for a V_{GS} between 0 and 3 V, in steps of 0.5 V. Figure 4c shows the transfer characteristics of the same transistors for V_{DS} = –2.5 V. The ON current is 3.8 mA at an operation voltage of 3 V, the estimated field-effect mobility in the saturation regime is 1.0 $cm^2 V^{-1}s^{-1}$.The threshold voltage is –1.0 V, and the ON/OFF ratio larger than 10^5.

2.3. Static and Dynamic Characteristics of an Organic SRAM Cell

Each memory cell of the SRAM array is comprised of five organic transistors. The circuit diagram and optical microscopy image can be seen in **Figure 5**a. All five TFTs have a channel length L of 20 µm; the channel width W is 3200 µm for the access TFT and the drive TFTs and 100 µm for the load TFTs. The area of one memory cell is 29 mm × 45 mm.

For the TFTs in the SRAM cells, the duration of the oxygen plasma treatment was set to 30 min, because the SRAM design requires depletion-mode transistors, i.e., the p-type DNTT TFTs must have a positive threshold voltage. The output and transfer characteristics of a drive TFT (W = 3200 µm) and of a load TFT (W = 100 µm) are shown in Figure S5. Both TFTs exhibit mobility of 1.5 cm^2/Vs. The threshold voltage is –0.02 V for the drive TFT and –0.15 V for the load TFT.

Figure 5b shows the static transfer characteristics of the two inverters of an SRAM cell for V_{DD} = 2 V, V_{BIAS} = –2 V, V_{SS} = 0 V. As can be seen, the two inverter characteristics are almost identical, and the small-signal gain is greater than 4. The SRAM butterfly curve is shown in Figure 5c. The static noise margin (SNM) extracted from the butterfly curve is 0.44 V. Figure 5d and e show the waveforms measured at the DATA and DATAb nodes during a write operation when the low state (0 V) is written from the bit line (BL) into the cell (Figure 5d), and during a write operation when the high state (2 V) is written from the bit line into the cell (Figure 5e). The write operations are initiated by changing the potential on the word line (WL) from 2 V (access transistor in the off-state) to –2 V (access transistor in the on-state), which causes the DATA and DATAb signals to flip. During the write operation shown in Figure 5d, when the low state is written into the cell, the DATAb transition time is 0.3 ms, while during the write operation shown in Figure 5e, when the high state is written, the DATAb transition time is 1.5 ms. Compared with our previous report on flexible organic SRAM arrays in which the organic TFTs were

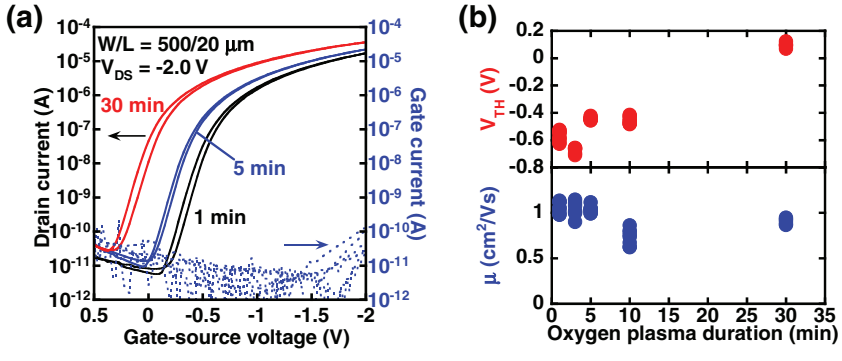

Figure 3. Threshold voltage control at different oxygen plasma durations: a) Transfer characteristics of DNTT TFTs for different durations of the oxygen plasma treatment performed to create the AlO_x layer (1 min, 5 min, 30 min). Solid lines: drain current; dotted lines: gate current. b) Threshold voltage and field-effect mobility in the saturation regime as a function of the oxygen plasma duration in the manufacturing process.

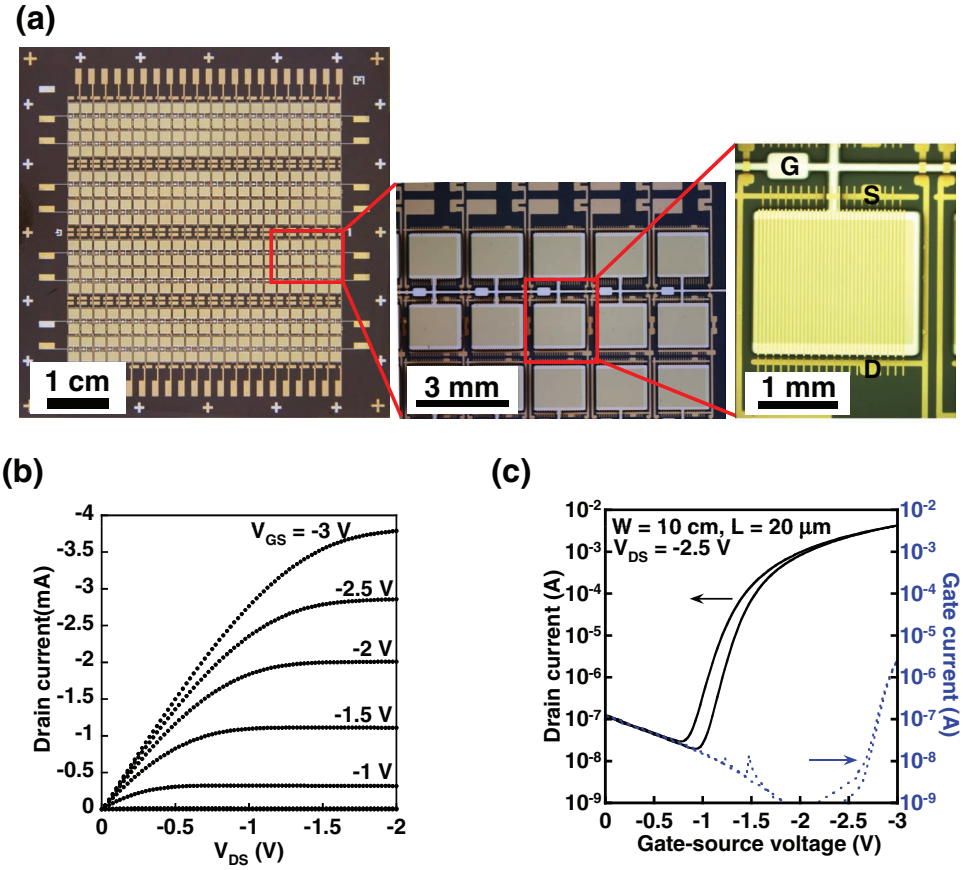

Figure 4. Operation of the integrated Braille display: a) A picture of an organic transistor active matrix. b) Output characteristics of a high-current organic TFT employed to drive a Braille dot. c) Transfer characteristics of the corresponding TFT. The TFT has a channel-width/channel-length (W/L) ratio of 5000 and provides a maximum current of more than 3 mA at 3 V. The mobility at the saturation regime is 1.0 $cm^2\ V^{-1}s^{-1}$, and the ON/OFF ratio exceeds 10^5.

fabricated using a thick polyimide gate dielectric and pentacene as the semiconductor,[28] the transition time of our new SRAM design based on low-voltage DNTT TFTs is 25 times faster.

2.4. Integrated Characteristics of One CNT-Based Actuator With Control TFTs, and Organic SRAM

One actuator with a size of 1 mm × 4 mm integrating with one TFTs driver and one TFTs SRAM was characterized. The displacement of the CNT-based actuator was also measured in air using a laser displacement meter and an oscilloscope. **Figures 6**a and b show voltages measured at the DATAb node and actuator's displacement as a function of time after the SRAM word line potential was changed from 3 V to –2 V. When voltages of the word line is changed from 3 to –2 V at t = 0, the DATAb signal is pulled from a large positive voltage (approximately equal to V_{DD}) down to 0 V, which causes the control TFT to turn on, which in turn causes the actuator and the Braille dot to move upward. For the bias condition $V_{DD} = V_{PL} = -4$ V, a displacement of 300 µm was measured, which is large enough for a blind person to recognize. The time required to produce a displacement of 300 µm is 6 s at $V_{DD} = V_{PL} = -4$ V and 2.9 s at $V_{DD} = V_{PL} = -4.5$ V.

The operating speed of the actuators is limited by the time required to charge and discharge the actuator electrodes. In order to obtain a faster response of the actuation, it is very important to increase the magnitude of the current flow from TFTs driver to actuators. Indeed, the operating speed of the actuators increases as the operating voltage of the TFTs driver is increased (Figure 6b). Therefore, the use of DNTT as p-type semiconductors and large W/L ratio of the TFTs driver facilitates the increase in the response time of the actuators.

3. Discussion

The DNTT TFTs exhibit very good air stability because of the large ionization potential of DNTT (5.4 eV).[30,31,33] Transfer characteristics as well as threshold voltage, mobility, and on/off ratio were essentially unchanged after the devices were exposed to ambient air for 170 days (Figure S4).

Not only the magnitude of the displacement, but also the dispersion of the displacement of the actuators is important to recognize correctly whether the individual dots are up or down. The SAM dielectrics can be formed quite uniform layers without any technical control,[23] so the dispersion of the TFTs using SAM as dielectrics will be very small.[23] Indeed, the

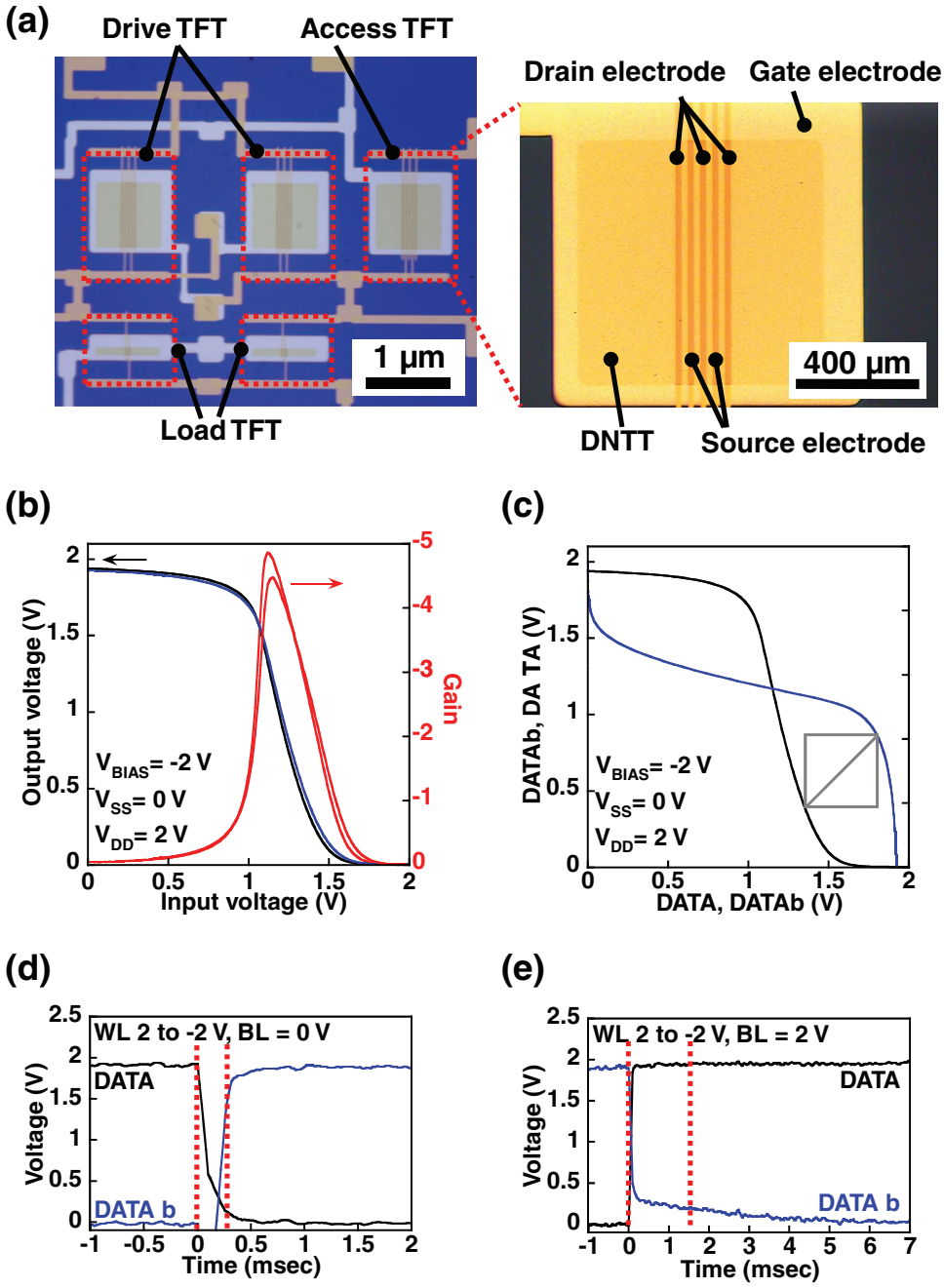

Figure 5. Static and dynamic characteristics of an organic SRAM cell. a) Optical microscopy image of an organic SRAM cell. The minimum feature size is 20 μm. b) Static transfer characteristics of the two inverters of an SRAM cell. c) Butterfly curve of an SRAM cell. The static noise margin extracted from the curve is 0.44 V. d) Measured DATA and DATAb waveforms during a write operation with a low bit line (BL) signal (0 V). The programming time, taken as the time until DATAb reaches 90% of the target potential, is 0.3 ms. e) Measured DATA and DATAb waveforms during a write operation with a high bit line signal (2 V). The programming time, taken as the time until DATAb reaches 90% of the target potential, is 1.5 ms.

control TFTs showed large current and low leakage current even though the TFTs have quite large channel width and very thin gate dielectrics less than 10 nm. This result demonstrates the high insulation property and the high uniformity of the SAM dielectrics. Furthermore, it is reported that the TFTs using DNTT as organic semiconductors have high air stability,[31] so the present device can be operational in the air conditions for a long time.

Previous works for organic and/or molecular memories were motivated for realizing cost-effective, high-density media memories. For this reason, almost all organic memories reported thus far are non-volatile memories: e.g., organic ferroelectric random access memory (FeRAM),[4–7] resistance random access memory (ReRAM),[8,9] and charge trap memory.[10] In addition to intensive efforts toward cheap organic memories, another trend is attempting to fully utilize the unique features

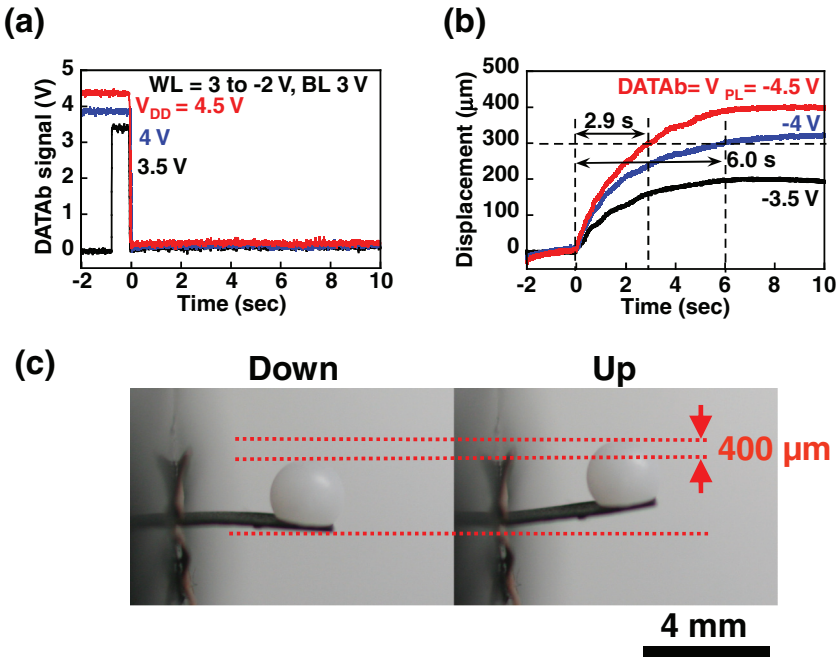

Figure 6. Operation of the integrated Braille display. a) Potential measured at the DATAb node as a function of time after the potential on the word line (WL) was changed from 3 to –2 V at t = 0, for three different supply voltages V_{DD}. b) Displacement of the actuator as a function of time for three different supply voltages V_{DD} and V_{PL} of –3.5, –4, and –4.5 V. The actuator has an area of 1 mm × 4 mm. c) Photographs of the actuator with a white Braille dot in the two static states (up and down).

of organic memories, such as mechanical flexibility and the ease of fabrication over large areas. Examples of new applications include sheet-type Braille displays and communication systems; both are possible by distributing organic memories over a large area.[6,11,12,28] In these applications, the critical feature required for organic memories is not non-volatility or high density but a faster programming speed.

Commercial silicon-based SRAM usually employs a complementary (CMOS) design, because complementary circuits have larger noise margins and lower power consumption than unipolar (PMOS) circuits. However, in the case of organic SRAM, complementary designs have a number of problems associated with the low field-effect mobility and poor air stability of organic n-channel TFTs,[34,35] which is the reason why we chose to implement a PMOS, rather than a complementary, SRAM.

Compared with the previously reported organic SRAM,[28] we achieved simultaneous reductions in operation voltage (from 40 V to 2 V) and programming time (from 40 ms to 2 ms). These substantial improvements are due to the high capacitance of the gate dielectric based on oxygen-plasma-grown AlO_x and a SAM of n-tetradecylphosphonic acid, and the large field-effect mobility of the organic semiconductor DNTT. Indeed, the same combination of AlO_x/SAM gate dielectric and DNTT has led to the realization of organic ring oscillators with a signal delay per stage of 37 µs at 3 V.[31]

In addition to the high mobility, good uniformity, and good air stability of the organic TFTs, the systematic control of the threshold voltage, which was demonstrated in this study, was critical for the low-voltage SRAM design. The threshold-voltage control provided a good balance for the switching characteristics of the inverters in the organic SRAM, so that a large static noise margin (SNM) of 0.44 was obtained at fairly low operating voltages without the necessity for a double-gate process.[28,36]

The main motivation for integrating each actuator of the Braille display with a memory cell is to reduce the time required to address a large number of Braille dots. If an individual Braille dot is controlled only by a transistor, then the time to produce a displacement of 300 µm is 1.8 s at 4 V, as shown in Figure S6. For a display composed of 144 Braille dots (12 × 12 array), the time to change all Braille dots (T_{all}) would thus be 21.6 s. When the SRAM array is added, T_{all} is the sum of the time required to program all 144 cells of the SRAM array plus the time required to change one Braille dot. Therefore, T_{all} is reduced to 2.91 s, because all 144 Braille dots are actuated simultaneously once the data are written into the SRAM array. Although the operating speed for a single actuator controlled by a transistor and an SRAM cell is slightly slower than the operating speed for a single actuator controlled only by a transistor, the fast SRAM programming speed (1.5 ms) enables a fast response of the Braille dot array.

In principle, the Braille display may be realized using an alternative memory concept, such as charge-trap memory or dynamic random access memory (DRAM). The main drawback of organic charge-trap memories is that they usually require either a large programming voltage or a long programming time (e.g., 6 V and 1 s, as in reference 9). The main problem with organic DRAM is that the rate at which the charge leaks away from the capacitor would be higher than the maximum possible refresh rate. Therefore, organic SRAM is a unique solution to achieve fast programming speeds and low programming

voltages simultaneously. A typical drawback of SRAM is the relatively large area requirement, due to the large number of devices per memory cell. However, unlike in silicon technology, where real estate is very expensive, the integration density in flexible large-area electronics applications is much smaller, so that the large area of SRAM is not really a drawback here.

Supporting Information

Supporting Information is available from the Wiley Online Library or from the author.

Acknowledgements

This study was partially supported by JST/CREST, NEDO, Special Coordination Funds for Promoting Science and Technology, and the Global COE Program on Physical Sciences Frontier, MEXT Japan.

Received: July 5, 2011
Published online: September 19, 2011

[1] D. Gebeyehu, C. J. Brabec, F. Padinger, T. Fromherz, J. C. Hummelen, D. Badt, H. Schindler, N. S. Sariciftci, *Synth. Met.*, **2001**, *118*, 1.
[2] B. Crone, A. Dodabalapur, Y.-Y. Lin, R. W. Filas, Z. Bao, A. LaDuca, R. Sarpeshkar, H. E. Katz, W. Li, *Nature* **2000**, *403*, 521.
[3] T. Someya, Y. Kato, T. Sekitani, S. Iba, Y. Noguchi, Y. Murase, H. Kawaguchi, T. Sakurai, *Proc. Natl. Acad. Sci. USA* **2005**, *102*, 12321.
[4] C. A. Nguyen, S. G. Mhaisalkar, J. Ma, P. S. Lee, *Org. Electron.* **2008**, *9*, 1087.
[5] K. H. Lee, G. Lee, K. Lee, M. S. Oh, S. Im, *Appl. Phys. Lett*, **2009**, *94*, 093304.
[6] T. Sekitani, K. Zaitsu, Y. Noguchi, K. Ishibe, M. Takamiya, T. Sakurai, T. Someya, *IEEE Trans. Electron Devices* **2009**, *56*, 1027.
[7] K. Zaitsu, S. Lee, K. Ishibe, T. Sekitani, T. Someya, *J. Appl. Phys.* **2010**, *107*, 114506.
[8] K. Asadi, D. M. de Leeuw, B. de Boer, P. W. M. Blom, *Nat. Mater.* **2008**, *7*, 547.
[9] J. Ouyang, C. W. Chu, C. R. Szmanda, L. Mai, A. Yang, *Nat. Mater.* **2004**, *3*, 918.
[10] T. Sekitani, T. Yokota, U. Zschieschang, H. Klauk, S. Bauer, K. Takeuchi, M. Takamiya, T. Sakurai, T. Someya, *Science* **2009**, *326*, 1516.
[11] T. Sekitani, M. Takamiya, Y. Noguchi, S. Nakano, Y. Kato, T. Sakurai, T. Someya, *Nat. Mater.* **2007**, *6*, 413.
[12] Y. Kato, T. Sekitani, M. Takamiya, M. Doi, K. Asaka, T. Sakurai, T. Someya, *IEEE Trans. Electron Devices* **2007**, *54*, 202.
[13] N. Fujiwara, K. Asaka, Y. Nishimura, K. Oguro, E. Torikai, *Chem. Mater.*, **2000**, *12*, 1750.
[14] K. Fukuda, T. Sekitani, T. Someya, *Appl. Phys. Lett.* **2009**, *95*, 023302.
[15] K. Mukai, K. Asaka, T. Sugino, K. Kiyohara, I. Takeuchi, N. Terasawa, D. N. Futaba, K. Hata, T. Fukushima, T. Aida, *Adv. Mater.* **2009**, *21*, 1582.
[16] S. Y. Yang, S. H. Kim, K. Shin, H. Jeon, C. E. Park, *Appl. Phys. Lett.* **2006**, *88*, 173507.
[17] M. E. Roberts, S. C. B. Mannsfeld, N. Queraltó, C. Reese, J. Locklin, W. Knoll, Z. Bao, *Proc. Natl. Acad. Sci. USA* **2008**, *105*, 12134.
[18] S. A. DiBenedetto, D. Frattarelli, M. A. Ratner, A. Facchetti, T. J. Marks, *J. Am. Chem. Soc.* **2008**, *130*, 7528.
[19] M. H. Yoon, A. Facchetti, T. J. Marks, *Proc. Natl. Acad. Sci. USA* **2005**, *102*, 4678.
[20] M. Kitamura, Y. Arakawa, *Appl. Phys. Lett.* **2007**, *91*, 053505.
[21] A. L. Deman, J. Tardy, *Org. Electron.* **2005**, *6*, 78.
[22] J. Ho Cho, J. Lee, Y. Xia, B. Kim, Y. He, M. J. Renn, T. P. Lodge, C. D. Frisbie, *Nat. Mater.* **2008**, *7*, 900.
[23] H. Klauk, U. Zschieschang, J. Pflaum, M. Halik, *Nature* **2007**, *445*, 745.
[24] T. Sekitani, Y. Noguchi, U. Zschieschang, H. Klauk, T. Someya, *Proc Natl. Acad. Sci. USA* **2008**, *105*, 4976.
[25] K. Fukuda, T. Hamamoto, T. Yokota, T. Sekitani, U. Zschieschang, H. Klauk, T. Someya, *Appl. Phys. Lett.* **2009**, *95*, 203301.
[26] K. Fukuda, T. Yokota, K. Kuribara, T. Sekitani, U. Zschieschang, H. Klauk, T. Someya, *Appl. Phys. Lett.* **2010**, *96*, 053302.
[27] T. C. Huang, K. Fukuda, C. M. Lo, Y. H. Yeh, T. Sekitani, T. Someya, K. T. Cheng, *IEEE Trans. Electron Devices* **2011**, *58*, 141.
[28] M. Takamiya, T. Sekitani, Y. Kato, H. Kawaguchi, T. Someya, T. Sakurai, *IEEE J. Solid-State Circuits* **2007**, *42*, 93.
[29] U. Kraft, U. Zschieschang, F. Ante, D. Kälblein, C. Kamella, K. Amsharov, M. Jansen, K. Kern, E. Weber, H. Klauk, *J. Mater. Chem.* **2010**, *20*, 6416.
[30] S. Haas, Y. Takahashi, K. Takimiya, T. Hasegawa, *Appl. Phys. Lett.* **2009**, *95*, 022111.
[31] U. Zschieschang, T. Yamamoto, K. Takimiya, H. Kuwabara, M. Ikeda, T. Sekitani, T. Someya, H. Klauk, *Adv. Mater.* **2010**, *22*, 982.
[32] Y. T. Tao, *J. Am. Chem. Soc.* **1993**, *115*, 4350.
[33] K. Takimiya, T. Yamamoto, H. Ebata, T. Izawa, *Sci. Technol. Adv. Mater.* **2007**, *8*, 273.
[34] Z. Bao, A. J. Lovinger, J. Brown, *J. Am. Chem. Soc.* **1998**, *120*, 207.
[35] M. M. Ling, Z. Bao, *Org. Electron.* **2006**, *7*, 568.
[36] S. Iba, T. Sekitani, Y. Kato, T. Someya, H. Kawaguchi, M. Takamiya, T. Sakurai, S. Takagi, *Appl. Phys. Lett.* **2005**, *87*, 023509.

Supporting Information

A 4 V operation, flexible Braille display using organic transistors, carbon nanotube actuators, and organic SRAM

Kenjiro Fukuda[1§], Tsuyoshi Sekitani[2], Ute Zschieschang[3], Hagen Klauk[3], Kazunori Kuribara[1], Tomoyuki Yokota[1], Takushi Sugino[4], Kinji Asaka[4], Masaaki Ikeda[5], Hirokazu Kuwabara[5], Tatsuya Yamamoto[6], Kazuo Takimiya[6], Takanori Fukushima[7], Takuzo Aida[8], Makoto Takamiya[9], Takayasu Sakurai[10],

Takao Someya[1,2,11,12]*

[1]Department of Applied Physics, The University of Tokyo, 7-3-1 Hongo, Bunkyo-ku, Tokyo 113-8656, Japan

[2]Department of Electrical and Electronic Engineering, The University of Tokyo, 7-3-1 Hongo, Bunkyo-ku, Tokyo 113-8656, Japan

[3]Max Planck Institute for Solid State Research, Heisenbergstr. 1, 70569 Stuttgart, Germany

[4]Research Institute for Cell Engineering, National Institute of Advanced Industrial Science and Technology (AIST), Midorigaoka 1-8-31, Ikeda, Osaka 563-8577, Japan

[5]Functional Chemicals R&D Laboratories, Nippon Kayaku Co., Ltd. 3-26-8, Shimo, Kita-ku, Tokyo, 115-8588, Japan

[6]Department of Applied Chemistry, Hiroshima University, 1-4-1, Kagamiyama,

Higashi-Hiroshima,Hiroshima, 739-8527, Japan

[7]Functional Soft Matter Engineering Laboratory, Advanced Science Institute, RIKEN, 2-1 Hirosawa,Wako, Saitama, 351-0198, Japan

[8]Department of Chemistry and Biotechnology, The University of Tokyo, 7-3-1, Hongo, Bunkyo-ku, Tokyo, 113-8656, Japan

[9]VLSI Design & Education Center, The University of Tokyo, 4-6-1, Komaba, Meguro-ku, Tokyo, 153-8505, Japan

[10]Institute of Industrial Science, The University of Tokyo, 4-6-1, Komaba, Meguro-ku, Tokyo, 153-8505, Japan

[11]Institute for Nano Quantum Information Electronics, The University of Tokyo, 4-6-1, Komaba, Meguro-ku, Tokyo, 153-8505, Japan

[12]Core Research for Evolutional Science and Technology, Sanban-cho Bldg, 4F, 5, Sanban-cho, Chiyoda-ku, Tokyo, 102-0075 Japan

§ Presently, Research Center for Organic Electronics, Yamagata University, 4-3-16, Jonan, Yonezawa, Yamagata, 992-8510, Japan

Correspondence and requests for materials should be addressed to T.S. (Takao Someya), someya@ee.t.u-tokyo.ac.jp

Department of Electrical and Electronic Engineering, School of Engineering, the University of Tokyo

7-3-1 Hongo, Bunkyo-ku, Tokyo 113-8656, JAPAN

Telephone: +81-3-5841-6756 Fax: +81-3-5841-6709

1. Carbon nanotube (CNT) based actuator (Fig. S1-S3)

1.1 Fabrication process (Fig. S1, S2)

The manufacturing process and pictures are shown in Fig. S1. Detailed explanations of the process flow may be found in the main text. As shown in the figures, the CNTs and polymers were uniformly dispersed in the solvents through the processes of stirring with an ionic liquid. Fig. S2 shows a cross-sectional image taken using scanning electron microscope (SEM, S4800, Hitachi high-technologies), where interfaces between electrodes and electrolytes in the CNT based actuators can be seen. After the pressure bonding process with heating at 70 °C, the polymer the polymers in the three layers were connected over the layer though the CNTs did not penetrate from electrode to the electrolyte.

1.2 Mechanical characteristics (Fig. S3)

We measured displacements of the actuator using laser displacement meter (KEYENCE, LE-4000) and an oscilloscope (Agilent, DSO6054A). Figure S3 shows the displacement as a function of time. CNT actuators with different thicknesses of 109 μm, 265 μm, and 456 μm can be seen Figs.S3a, b, and c, respectively. The actuator size was 1×4 mm^2. The input voltage changed from ±2.0 V to ±3.0 V. For all actuators, the displacement increased as increasing the input voltage from ±2.0 V to ±3.0 V. For the actuator whose thickness was 109 μm, the displacement increased from 250 to 720 μm as increasing the

input voltage from ±2.0 V to ±3.0 V. These results indicate the displacement of the actuator can be controlled by changing operational voltages and the thickness.

2. Air stability of DNTT TFTs (Fig. S4)

Figure S4a shows current–voltage characteristics of a DNTT TFT on a Si/SiO_2 substrate measured immediately after exposure to ambient air. The TFT exhibited a mobility of 1.3 cm^2/Vs, a threshold voltage of –0.3 V, and an on/off current ratio of 10^5. Figure S4b shows the characteristics of the same transistor measured after 6 months (170 days) stored in ambient air; whose mobility is 1.4 cm^2/Vs, threshold voltage is –0.26 V, and on/off current ratio is 10^5. Figure S4c shows changes in threshold voltage, mobility, and on/off ratio as time passed in air. The TFT characteristics are almost the same even after 170 days in air, which indicates the excellent air stability of the DNTT p-channel TFTs.

3. Electrical characteristics of organic SRAM (Fig. S5, S6)

3.1 Output characteristics of DNTT TFTs in an SRAM cell (Fig. S5)

The output characteristics of the drive and load TFTs in an SRAM cell are shown in Figure S5a and b, respectively. These pictures can be seen in Fig. 5 in the main text. The drain current I_D was measured as a function of the drain-source voltage V_{DS} for gate-source voltages V_{GS} between 0 to –2 V in steps of 0.5 V. We found a linear increase in drain current I_D at small V_{DS}, which indicates that the contact resistance between the DNTT semiconductor and the gold source/drain contacts is negligibly small.

3.2 Retention characteristic of the SRAM (Fig. S6)

A retention characteristic of the SRAM was measured in air. The measurement procedure was as follows: First, a voltage of –2 V was applied to the word line (WL) and then a voltage of -2 V or 0 V was applied to the bit line, to realize the Low state or the High state in the SRAM cell. Second, the WL was connected to 0 V. Finally, the supply voltage V_{DD} was kept constant at –2 V, and the voltage at DATAb was monitored. Figure S6 shows the of DATAb voltage over time. The stored information is stable for about 500 sec.

4. Displacement of CNT-based actuators with control TFTs (Fig. S7)

Figure S7a shows the schematic of an actuator integrated with organic TFT that can drive large channel currents. Figure S7b shows time-dependent displacement of the actuator having a size of 1 × 4 mm^2 when controlled by the TFT. A square-wave signal with an amplitude of 2 V and a frequency of 0.1 Hz was applied to the drain contact of the TFT, and the displacement of the actuator was measured as a function of time for various TFT gate-source voltages (V_{GS}; ranging from –2.5 V to –4 V). The maximum displacement increases monotonically with increasing V_{GS}, from 210 μm at V_{GS} = –2.5 V to 450 μm at V_{GS} = –4 V. The time required to produce a displacement of 300 μm is 1.8 sec at V_{GS} = –4 V; under these bias conditions the current reaches a maximum of 3.9 mA.

5. Minimum frame time of a Braille display with 12 rows and 12 column (Fig. S8)

Figure S6 summarizes estimated time required to address 144 Braille dots arranged in 12 rows and 12 columns with and without the assistance of an organic SRAM array.

Without the SRAM array the 12 rows must addressed sequentially, i.e. one after the other. Addressing one row takes 1.8 sec (assuming a minimum displacement of 300 μm), so the total time required to address all 12 rows with all 144 dots (i.e., the frame time) is 21.6 sec. When the Braille dot array is equipped with an SRAM array, all the data are first programmed into the SRAM array and then all 144 Braille dots are addressed simultaneously using the information stored in the SRAM array, so the frame time is significantly shorter, only 2.91 sec. This clearly shows the significant benefit of combining the Braille display with an SRAM array.

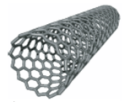

Carbon nanotube (CNT)
50 mg

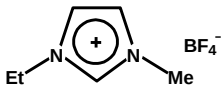

Ionic liquid (EMI-BF4)
120 mg

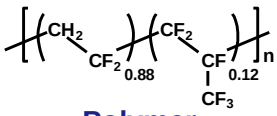

Polymer (PVDF-HFP)
80 mg

Stirr for 3 days, at room temperature with DMAc 4 ml
& Sonicate for 1 day

CNT disperased gel

Add DMAc 5 ml, then Stirr for 1 days, at room temperature
& Sonicate for 1 day

CNT disperased gel

Casting on 20 mm by 20 mm mold
Drying on hotplate, 50 °C for 1 day
then Vacuum oven, 80 °C for 3 days

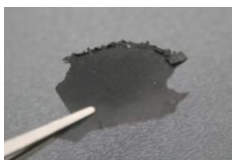

CNT electrode

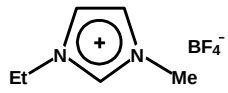

Ionic liquid (EMI-BF4)
100 mg

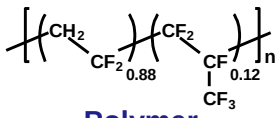

Polymer (PVDF-HFP)
100 mg

Stirr for 1 day, at 70 °C sandbath
with MP 3 ml and PC 0.25 g
& Sonicate for 1 day

Gelatinous mixture

Casting on 20 mm by 20 mm mold
Drying on hotplate, 50 °C for 1 day
then Vacuum oven, 80 °C for 3 days

Electrolyte

Press 90 N at 70 °C for 90 sec,
270 N at 70 °C for 90 sec

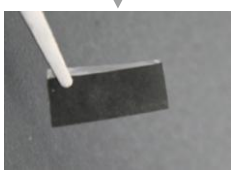

CNT-based actuator

Fukuda et al., Fig. S1

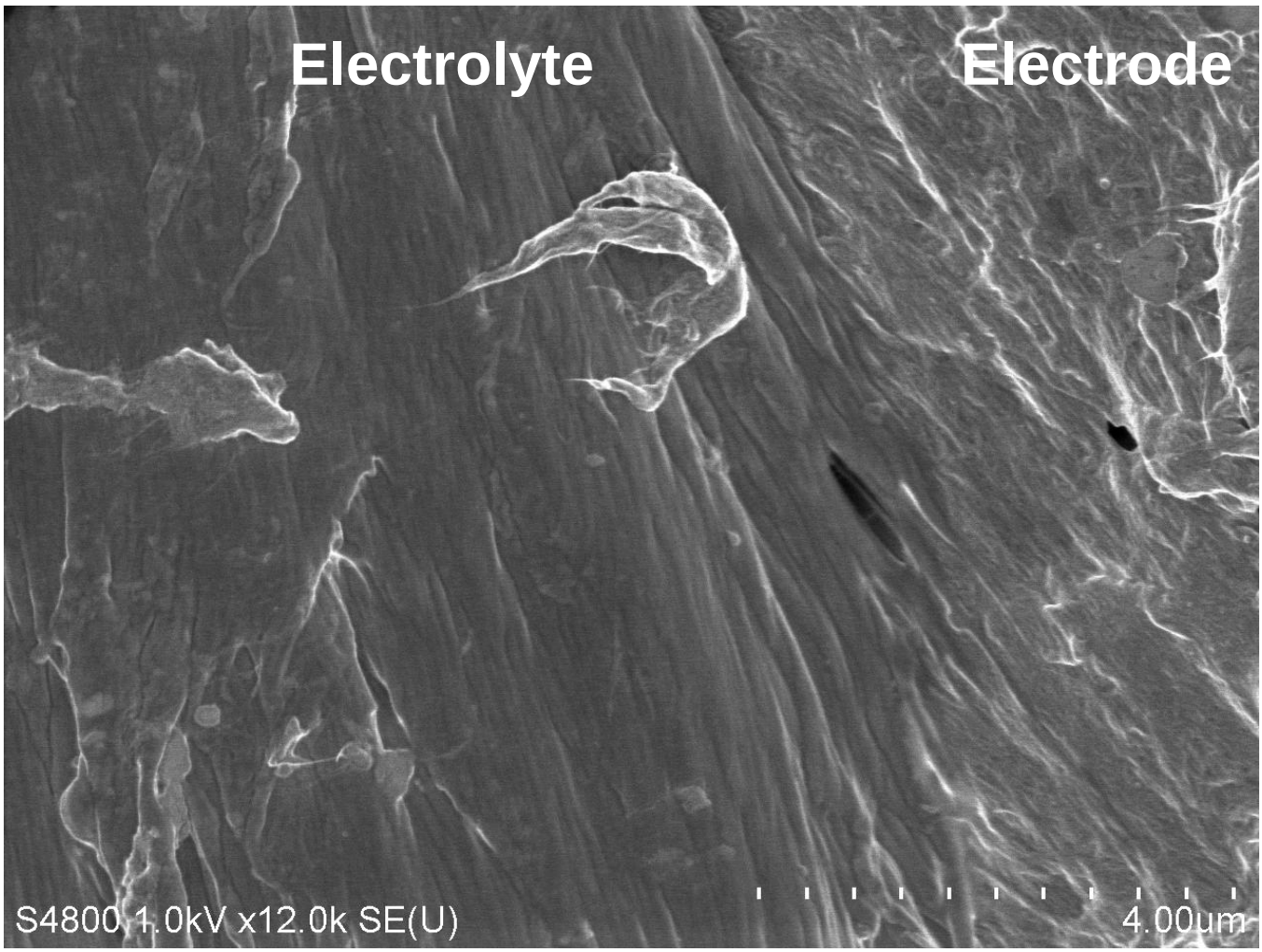

Fukuda et al., Fig. S2

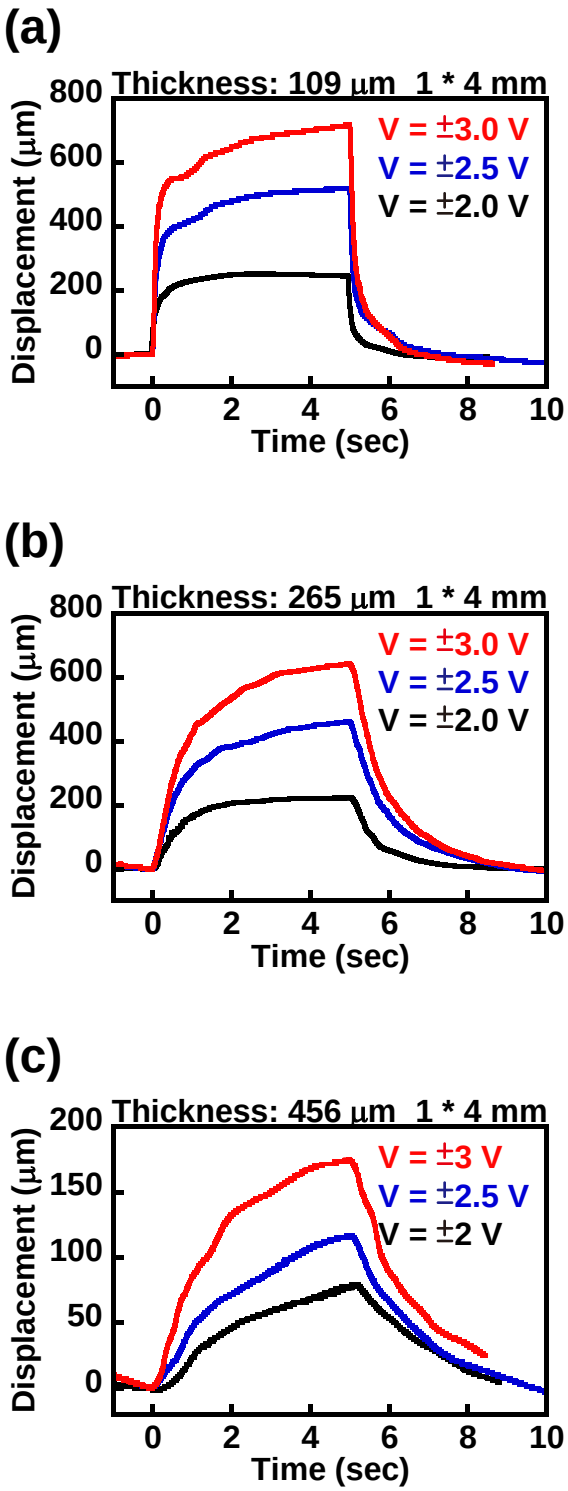

Fukuda et al., Fig. S3

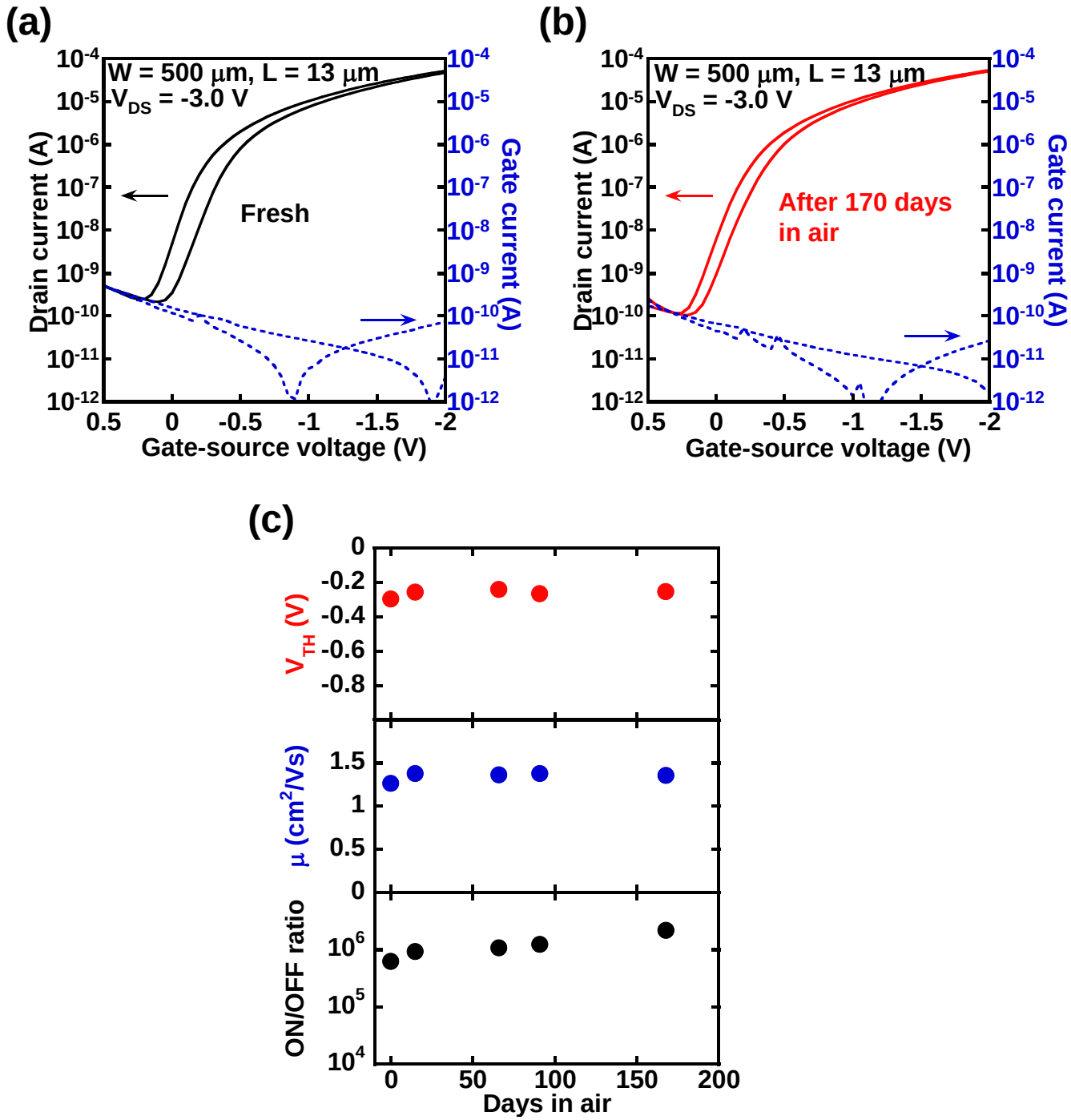

Fukuda et al., Fig. S4

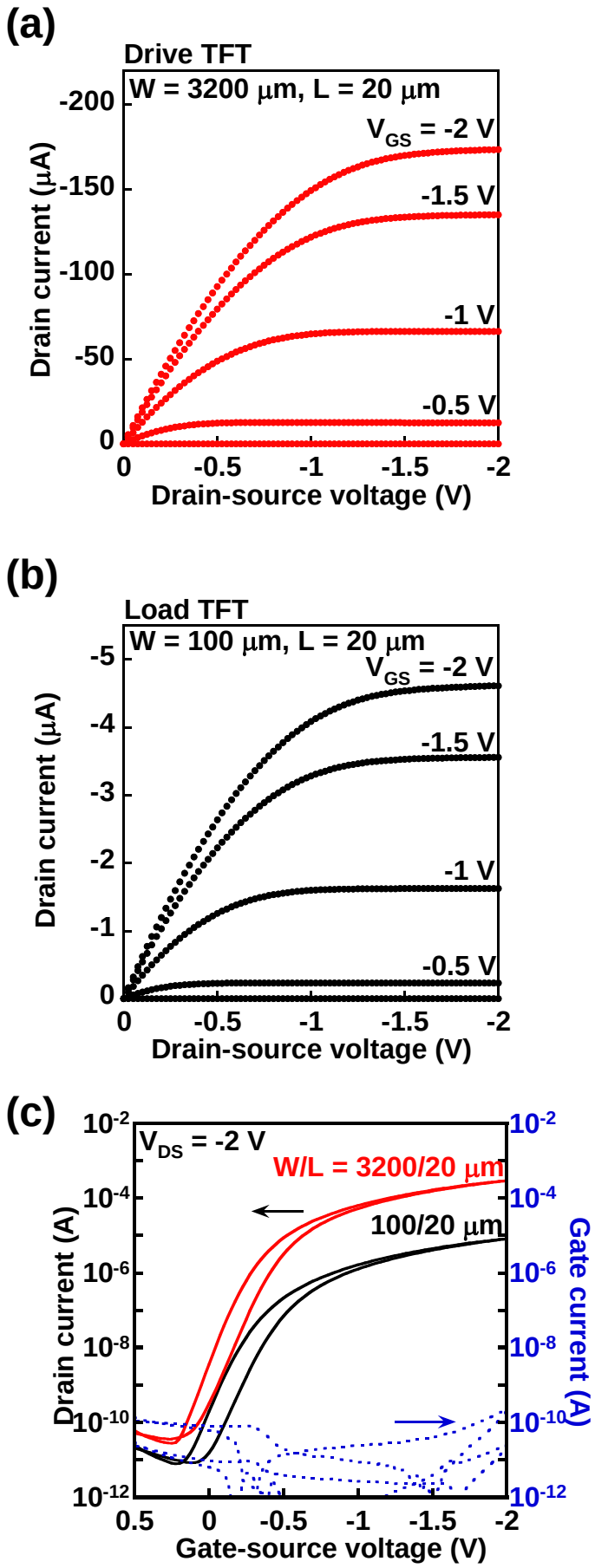

Fukuda et al., Fig. S5

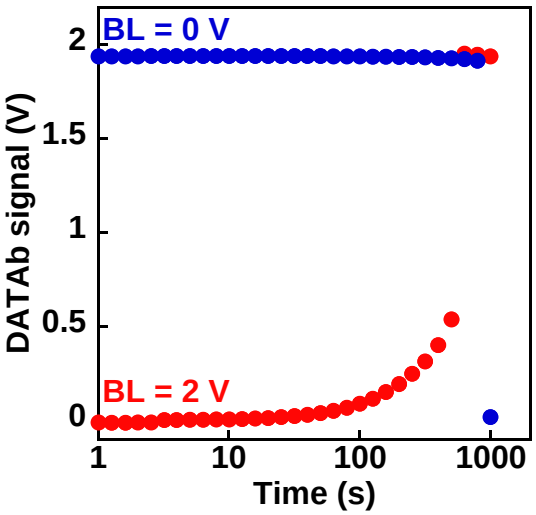

Fukuda et al., Fig. S6

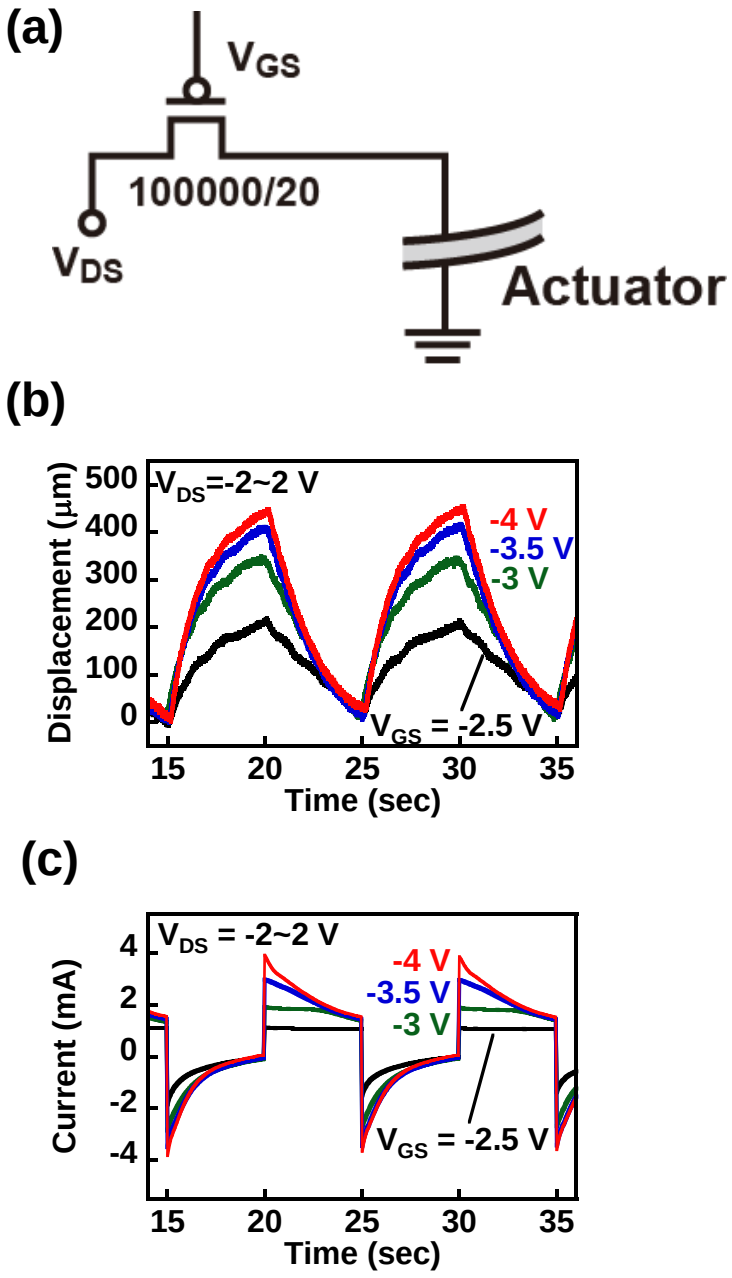

Fukuda et al., Fig. S7

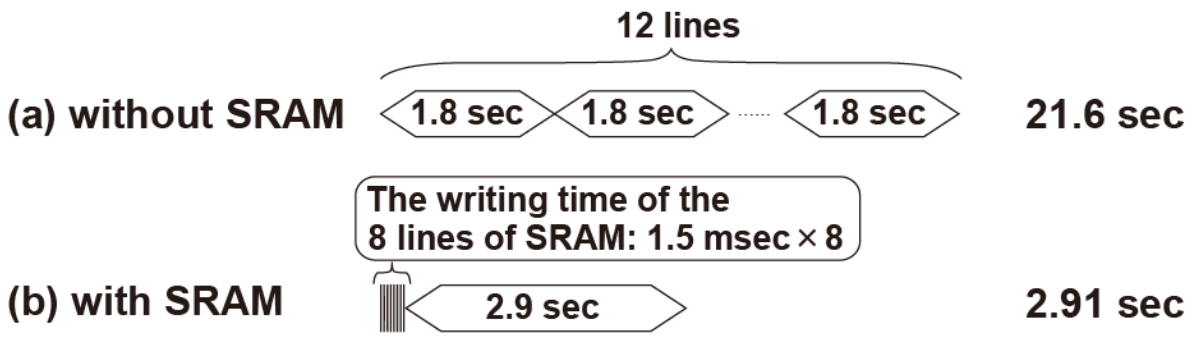

Fukuda et al., Fig. S8